Supplement of Atmos. Chem. Phys., 25, 1685–1709, 2025
https://doi.org/10.5194/acp-25-1685-2025-supplement
© Author(s) 2025. CC BY 4.0 License.

*Supplement of*

# Evaluation of the WRF-Chem performance for the air pollutants over the United Arab Emirates

**Yesobu Yarragunta et al.**

*Correspondence to:* Diana Francis (diana.francis@ku.ac.ae)

The copyright of individual parts of the supplement might differ from the article licence.

**Table S1** List of seven Automatic Weather Stations operated in airports —five land-based and two coastal—alongside the Wind-blown Sand Experiment (WISE) site and two AERONET stations, Mezaira and Dewa, for AOD assessment in the United Arab Emirates (UAE).

| Station Name | Metar code | Latitude | Longitude | Elevation (m) | Region |
|---|---|---|---|---|---|
| WISE-UAE | WISE | 23.58 | 53.72 | 119 | Land |
| Abu Dhabi | OMAA | 24.43 | 54.65 | 27 | Land |
| Abu Dhabi | OMAD | 24.43 | 54.46 | 3 | Coastal |
| Al Maktoum | OMDW | 24.90 | 55.16 | 19 | Land |
| Dubai | OMDB | 25.25 | 55.37 | 5 | Coastal |
| Sharjah | OMSJ | 25.33 | 55.52 | 33 | Land |
| Al Ain | OMAL | 24.26 | 55.61 | 262 | Land |
| Ras Al Khaimah | OMRK | 25.61 | 55.94 | 31 | Land |
| Mezaira | | 23.11 | 54.76 | 201 | Land |
| Dewa | | 24.77 | 55.37 | 88 | Land |

The WRF-Chem model effectively represents the observed variability in T2m, RH2m, and WS10m across all seven meteorological stations during June and December 2022. An inspection of Table S2 reveals the WRF-Chem model generally overestimates the observed T2m values by less than 0.8 °C in June and underestimates in December by less than 5.2 °C across most locations. Previous studies revealed a cold bias, more pronounced in the summer months (e.g., Branch et al., 2021; Chaouch et al., 2017; Fonseca et al., 2020; Temimi et al., 2020), which has been attributed to an incorrect representation of the aerosol loading, greenhouse gas concentrations and surface properties (e.g., very high surface emissivity values, as noted in Parajuli et al., 2023), and deficiencies in the physics schemes, in particular in the land surface, PBL and radiation schemes. The fact that the temperature bias is positive in the summer, and of a much reduced magnitude compared to that reported in other studies where it exceeds 3 °C (Branch et al., 2021; Temimi et al., 2020), stresses the importance of correctly representing the aerosol loading in this region, as noted by Fonseca et al. (2021). Correlation coefficients for the observed T2m with model simulations ae between 0.81 and 0.85 in June, slightly decreasing to a range of 0.79 to 0.81 in December. Lower correlation values in the December month likely arise from an incorrect simulation of the timing of the passage of mid-latitude baroclinic systems, which largely control the weather conditions in the region during the colder months (Nelli et al., 2022). The fact that even at 3 km the model will not be able to fully capture the complex land-sea mask may justify the slightly lower correlation values at coastal sites when compared to inland stations, as noted by Abida et al. (2022). The WS10m biases are also lower than those reported in other studies, typically by a factor of two to three, suggesting an overall improved representation of the boundary layer dynamics. As this field exhibits a more pronounced spatial and temporal variability compared to T2m, the correlation coefficients will be lower, with values in the range 0.3-0.4. The dry bias, noted by virtually all previous modeling studies in the region and more pronounced in the summer months (e.g., Branch et al., 2021; Temimi et al., 2020), is also present with this model configuration. Possible explanations include deficiencies in the representation of the soil moisture, which plays an important role in driving the atmospheric dynamics in the region (e.g. Francis et al., 2021; Wehbe et al., 2019), and an incorrect representation of the mesoscale land-sea breeze circulations (Fonseca et al., 2022; Gopalakrishnan et al., 2023; Temimi et al., 2020).

**Table S2 Statistical evaluation against UAE Airport station data:** skill scores for air temperature at 2m (T2m), wind speed at 10m (WS10m), and Relativity humidity at 2m (RH2m) for seven airport stations (categorized into land and coastal regions) over the UAE listed in Table S1.

| Parameter | **Month** | **Region** | **MOD** | **OBS** | **MB** | **MAE** | **RMSE** | R |
|---|---|---|---|---|---|---|---|---|
| T2m ($^o$C) | June | Land | 35.65 | 35.50 | 0.16 | 3.67 | 4.52 | 0.85 |
| | | Coastal | 35.66 | 35.42 | 0.24 | 4.48 | 5.34 | 0.81 |
| | Dec | Land | 19.03 | 22.36 | -3.32 | 3.90 | 4.65 | 0.86 |
| | | Coastal | 19.04 | 24.12 | -5.07 | 5.54 | 6.53 | 0.79 |
| WS10m (m/s) | June | Land | 3.98 | 4.03 | -0.05 | 2.03 | 2.58 | 0.25 |
| | | Coastal | 3.98 | 3.54 | 0.43 | 1.74 | 2.18 | 0.36 |
| | Dec | Land | 3.55 | 3.08 | 0.47 | 1.50 | 1.89 | 0.34 |
| | | Coastal | 3.55 | 3.06 | 0.49 | 1.43 | 1.78 | 0.42 |
| RH2m (%) | June | Land | 17.69 | 40.71 | -23.02 | 25.32 | 29.77 | 0.36 |
| | | Coastal | 17.68 | 46.96 | -29.28 | 31.21 | 35.48 | 0.29 |
| | Dec | Land | 52.32 | 62.44 | -10.12 | 15.70 | 19.11 | 0.63 |
| | | Coastal | 52.29 | 59.06 | -6.78 | 14.60 | 17.88 | 0.57 |

The WRF-Chem model performance has also been evaluated against WISE-UAE measurements for T2m, RH2m, WS10m, and SW for December 2022 (the experiment initiated in July 2022 so no data for June 2022), with the skill scores summarized in Table S3. By and large the model performance is similar to that found for the airport stations in Table S2. In particular, there is an underestimation of T2m by about 1.6 °C, and a slight overestimation of

WS10m by 0.78 m/s, and a negative bias in RH2m by about -17%. The higher correlation values at this inland barren site indicate a superior model skill in capturing the diurnal cycle in a rural environment as opposed to major urban airport areas, whose complexity will not be fully represented in WRF-Chem. The WRF model has shown a tendency to overestimate the observed wind speed across the country over all seasons (e.g., Branch et al. 2021; Fonseca et al. 2020, 2021, 2022b; Temimi et al., 2020), which has been put down to an incorrect representation of its subgrid-scale variability and deficiencies in the surface drag parameterization scheme. Additionally, the model overestimates SW by 29 W/m², even though it captures very well its diurnal cycle, as evident by the high correlation coefficient of 0.94. The positive bias in SW may be attributed to an underprediction of the observed cloud cover, as noted by Wehbe et al. (2019) and Fonseca et al. (2020, 2022a), which is the highest in the region in the colder months (Yousef et al., 2020).

**Table S3 Statistical evaluation against WISE-UAE measurements:** Skill scores for 2-meter air temperature (T2m), 10-meter wind speed (WS10m), 2-meter relative humidity (RH2m), and downward shortwave radiation flux (SW) at the WISE-UAE location in the UAE.

| **Parameter** | **MOD** | **OBS** | **MB** | **MAE** | **RMSE** | R |
|---|---|---|---|---|---|---|
| T2m ($^o$C) | 18.74 | 20.34 | -1.60 | 2.19 | 2.66 | 0.94 |
| WS10m (m/s) | 3.56 | 2.78 | 0.78 | 1.52 | 1.82 | 0.59 |
| RH2m (%) | 52.75 | 69.62 | -16.87 | 18.21 | 21.94 | 0.76 |
| SW (W/m$^2$) | 204.13 | 174.91 | 29.22 | 57.33 | 98.61 | 0.94 |

A more detailed analysis  is presented in Fig, S1(a), which shows the average diurnal variation in T2m from WRF-Chem simulations and observations for December 2022. The negative T2m bias seen in Table S3 arises mostly from cold nighttime temperatures, Fig. S1(a), as noted before and reported in previous studies (e.g., Abida et al., 2022; Branch et al., 2021; Fonseca et al., 2021; Schwitalla et al., 2020; Temimi et al., 2020), with the daytime temperatures simulated well by the model, generally within 1 °C. The sharp drop between 14-15 UTC (18-19 LT) occurs around the sunset, Fig. S1(d), at a time when the model's underestimation of the observed RH2m becomes more pronounced exceeding 20%, Fig. S1(c), and just before it starts overestimating the strength of the observed wind speed, Fig. S1(c). This is consistent with a stronger offshore flow in WRF-Chem, advecting the cooler and drier inland air into the WISE-UAE site.

Fig. S1(b) shows an overestimation of the observed wind speed at night, by up to 2 m/s, and a slight underestimation during daytime, by up to 1 m/s, indicating deficiencies in the representation of the nighttime PBL, as noted by Chaouch et al. (2017), Temimi et al. (2020) and Abida et al. (2022). The dry bias is more pronounced during nighttime hours, Fig. S1(c), arising from increased advection of drier air from the inland desert owing to a more offshore wind direction in the model (not shown). The underestimation of the observed cloud cover is evident in Fig. S1(d) by the smaller variability of the model-predicted SW and the overestimation of the observed magnitude by up to 100 W/m$^2$, the latter also reflecting deficiencies in the radiation scheme and an incorrect representation of the aerosol loading and greenhouse gas concentrations. The 1-h lag between the observed and WRF-Chem SW diurnal cycle has been noted by Weston et al. (2018). It may be explained by discrepancies between the modelled and observed aerosol loading, greenhouse gas concentration, surface properties and topography.

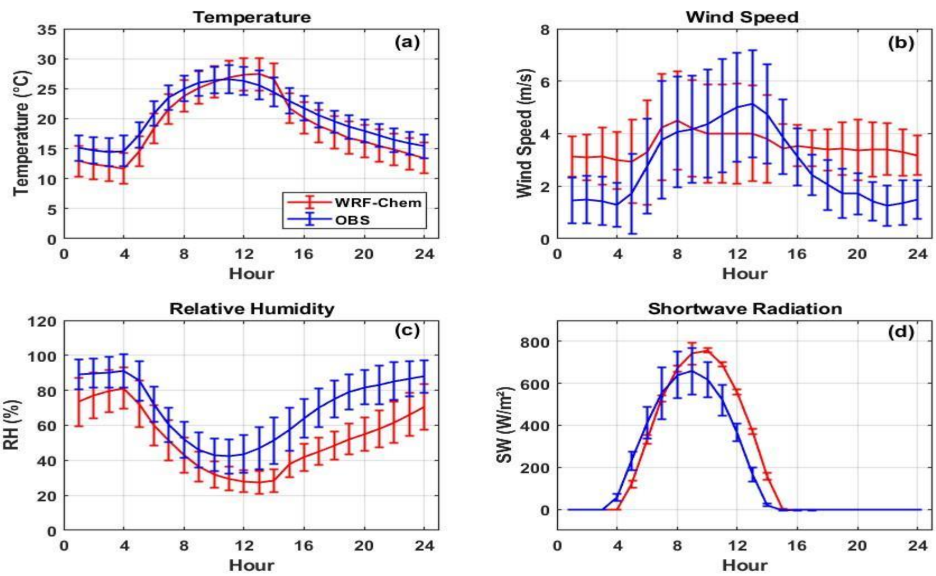

**Figure S1: WRF-Chem Evaluation at WISE-UAE Site for December 2022:** Diurnal cycle of monthly-mean values for WRF-Chem simulated (red) and observed (blue) air temperature at 2m (T2m, °C) in (a), wind speed at 10m (WS10m, m/s) in (b), relative humidity at 2m (RH2m, %) in (c), and downward shortwave radiation flux (SW, W/m²) in (d), for December 2022. The averaged spatial standard deviation is represented by error bars at each hour.

In Fig. S2, a spatial comparison is presented between the averaged ERA5 T2m and the corresponding WRF-chem simulation output across the simulation domain during June and December of 2022. The model adeptly captures regional temperature variations, displaying an underestimation in the south-western regions typically by 1-3°C and an overestimation in the north-eastern region of the UAE, by less than 1°C (Figs. S2(a)-(c) and (e)-(g)). A comparison with the statistics against the airport stations (Table S2) and the WISE-UAE field measurements (Table S3; Fig. S1) suggests the reanalysis dataset gives a good representation of the observed air temperature in both months, which has been noted by Nelli et al. (2024). WRF-Chem underestimates the area-averaged temperature (T2m) over the UAE compared to ERA5 in both seasons, Figs. S2(d) and (h). This is in contrast with the evaluation against the airport station data, which indicates an overestimation during the summer and an underestimation during the winter (Table S2). Kishta et al., (2023) reported minor discrepancies in temperature measurements between the observational data and ERA5 reanalysis, identifying a strong correlation coefficient of 0.89 over Abu Dhabi. This is further confirmed by Nelli et al. (2024), who found air temperature biases not exceeding 0.7 °C and correlation coefficients not lower than 0.92 for all seasons. The spatial average of the WRF-Chem and ERA5 values are 33.1 °C and 34.0 °C, respectively, with an underestimation of 1°C over the UAE. The model displays a high correlation (r) of 0.97 and a RMSE of 0.8 °C, MAE of 1.1 °C in June. For December, the model shows a similar pattern, with an underestimation of 0.9 °C, which is slightly lower compared to June, an r value of 0.92, a MAE of 1.0 °C and a RMSE of 1.1 °C (Table S4).

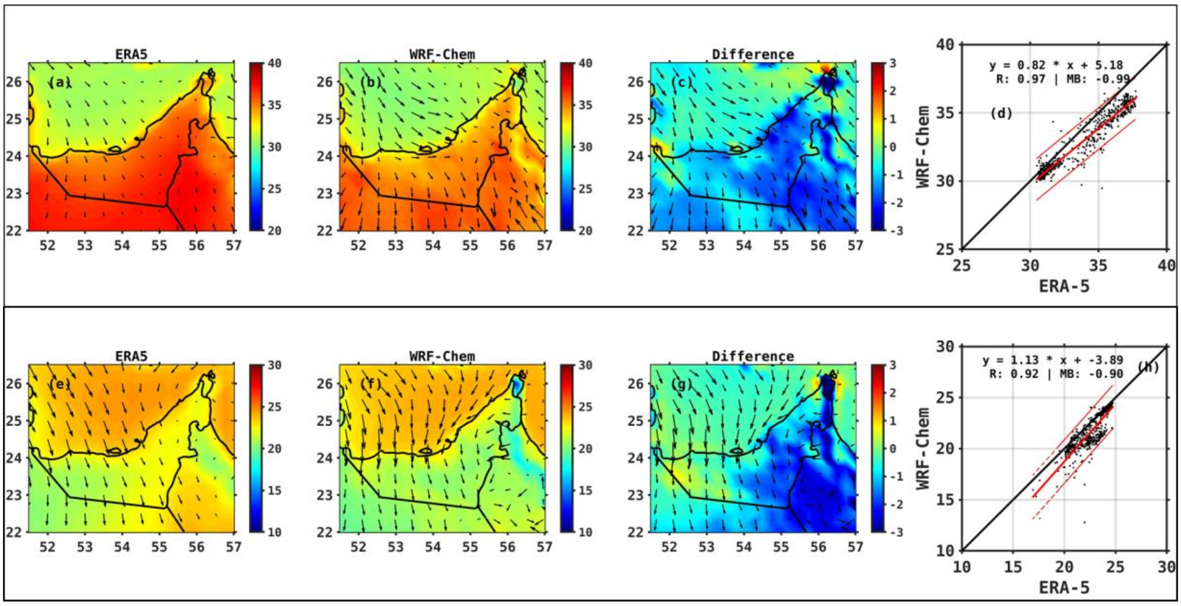


**Figure S2: ERA-5 and WRF-Chem Air Temperature:** Average 2-m air temperature (°C) obtained from ERA5 reanalysis (a,e), simulated by WRF-Chem (b,f), the corresponding absolute differences (c,g), and scatter plots between the two datasets (d,h) during June (top) and December (bottom) 2022. The 10m wind vectors are overlaid on the corresponding spatial plots.

It is widely recognized that the Planetary boundary layer (PBL) plays a crucial role in the advection and dispersion of pollution over the region (Phanikumar et al., 2020). The PBL is deeper during summer and shallower in winter (Nelli et al., 2021). There are noticeable differences in the PBL between land areas (approximately 2400–2500 m) and marine regions (about 1200–1500 m), as expected given the contrasting thermal inertia between the ocean water and the land surface . Basha et al. (2019) discovered that ERA-Interim reanalysis data tends to underestimate the PBL depth when compared with data obtained from Global Positioning System Radio Occultation (GPSRO) in most regions and in all the seasons. Chen et al. (2022) emphasized the critical role of the boundary layer in influencing air quality and facilitating the transboundary transport of pollutants. The authors noted that a deeper boundary layer enhances the potential for pollutant transport to the Tibetan Plateau. Wang et al. (2022) highlighted the critical role of meteorological conditions in severe $PM_{2.5}$ pollution episodes, stressing that rapid cold air advection can quickly disperse pollutants, in contrast to the slow accumulation of pollutants under weak high-pressure systems. This slow build-up is characterized by low wind speeds, and low atmospheric boundary layer heights, which lead to prolonged heavy pollution periods and potentially fog events given the aerosols' role in acting as cloud condensation nuclei (Pauli et al., 2024).

Fig. S3 shows a comparison of the mean ERA5 PBL with corresponding WRF-chem simulated values for the months of June and December 2022. The spatial distribution of PBL across the UAE, with higher values over land regions and lower values over the marine regions in the summer, Figs. 3(a)-(b), and the opposite in winter, Figs. 3(e)-(f), is seen in both ERA5 and WRF-Chem, and is consistent with the  seasonal temperature variations (cf. Figs S2(a)-(b) and (e)-(f)). In particular, warmer summer temperatures contribute to an elevation in PBL, and cooler winter temperatures are accompanied by lower PBL heights (Basha et al., 2019). It is surprising that over the Arabian Gulf the PBL is deeper in December than in June, cf. Figs. S3(a)-(b) but (e)-(f). This arises because of increased wind speeds and turbulent mixing in the colder months, which drive deeper PBLs (Dai, 2024). In terms of the model simulated PBL depths (averaged spatially for the UAE), WRF-Chem exhibits good performance in capturing the regional variations seen in the reanalysis dataset. In June, the modelled PBL is at 657 m compared to 606 m in ERA5, with a correlation coefficient of 0.98 and a RMSE of 232 m. In December, the modelled PBL is 516 m compared to the ERA5 of 526 m, with a high correlation coefficient of 0.98 and an RMSE of 136 m (Table S4). The good agreement between the WRF-Chem and ERA5's PBL depth suggests the model is capable of simulating the spatial and temporal variability of the PBL across the UAE in both seasons.

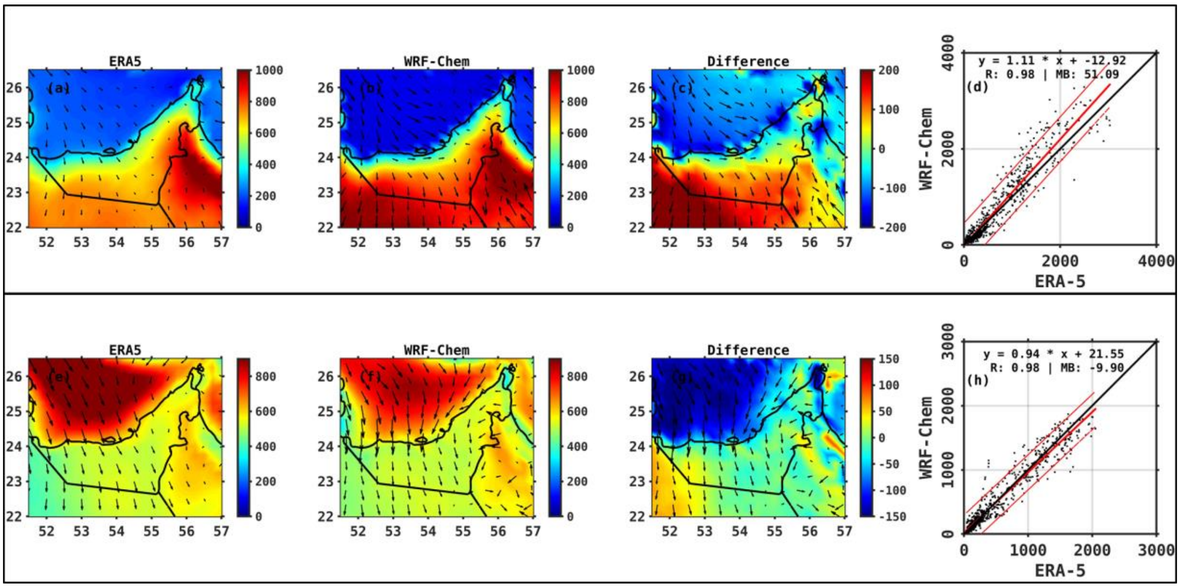


**Figure S3: ERA-5 and WRF-Chem Boundary Layer Height:** Same as Fig. S2, but for the planetary boundary layer (PBL) height.

In addition to T2m and PBL, Table S4 also summarizes the spatially averaged statistical verification scores for WS10m and SR over UAE. Regarding WS10m, it is accurately simulated by the model with small differences in MB (June: 0.6 m/s, Dec: 0.4 m/s), which are largely comparable to those obtained at the location of the airport stations (Table S2) and WISE-UAE location (Table S3), with good correlations in both seasons (June: 0.51, Dec: 0.88). This suggests the reanalysis dataset also overestimates the strength of the wind speed in the region, as noted by Nelli et al. (2024). These biases have been attributed to an incorrect representation of the near-surface wind subgrid-scale variability and deficiencies in the surface drag parameterization scheme employed in the model (Nelli et al., 2020; Temimi et al., 2020). The excessive SW in WRF-Chem seen with respect to the WISE-UAE field measurements (Table S4) is also seen with respect to ERA5 data in Table S5, with the reanalysis also exhibiting a tendency to overpredict the net shortwave radiation flux (Nelli et al., 2024). In any case, these results presented in Figs. S1-S3 and Tables S2-S4 indicate a very good performance of the WRF-chem model in simulating meteorological parameters over the UAE during the specified months with respect to both *in situ* observations and a state-of-the-art reanalysis dataset. Since WRF-Chem simulates meteorology and chemistry simultaneously, accurate meteorological simulations are crucial for the precise computation of chemistry fields within the model domain.

**Table S4 Statistical evaluation against ERA-5 data:** skill scores calculated for model simulations for air temperature at 2m (T2m), wind speed at 10m (WS10m), downward shortwave radiation flux (SW), and planetary boundary layer (PBL) during June and December of 2022 over the UAE.

| **Parameter** | **Month** | **MOD** | **ERA5** | **MB** | **MAE** | **R** | **RMSE** |
|---|---|---|---|---|---|---|---|
| T2m ($^{o}$ C) | June | 33.06 | 34.04 | -0.99 | 1.05 | 0.97 | 0.78 |
| | Dec | 21.87 | 22.76 | -0.90 | 0.95 | 0.92 | 1.06 |
| WS10m (m/s) | | 4.29 | 3.72 | 0.57 | 0.63 | 0.51 | 0.53 |
| | | 3.88 | 3.46 | 0.42 | 0.53 | 0.88 | 0.60 |
| SW (W/m$^2$) | | 350.2 | 309.0 | 41.3 | 41.3 | 0.94 | 1.9 |
| | | 188.1 | 172.2 | 15.9 | 15.9 | 0.99 | 2.6 |

| | | | | | | | |
|---|---|---|---|---|---|---|---|
| PBL (m) | | 656.8 | 605.8 | 51.1 | 101.8 | 0.98 | 231.9 |
| | | 516.0 | 525.9 | -10.0 | 91.2 | 0.98 | 136.3 |

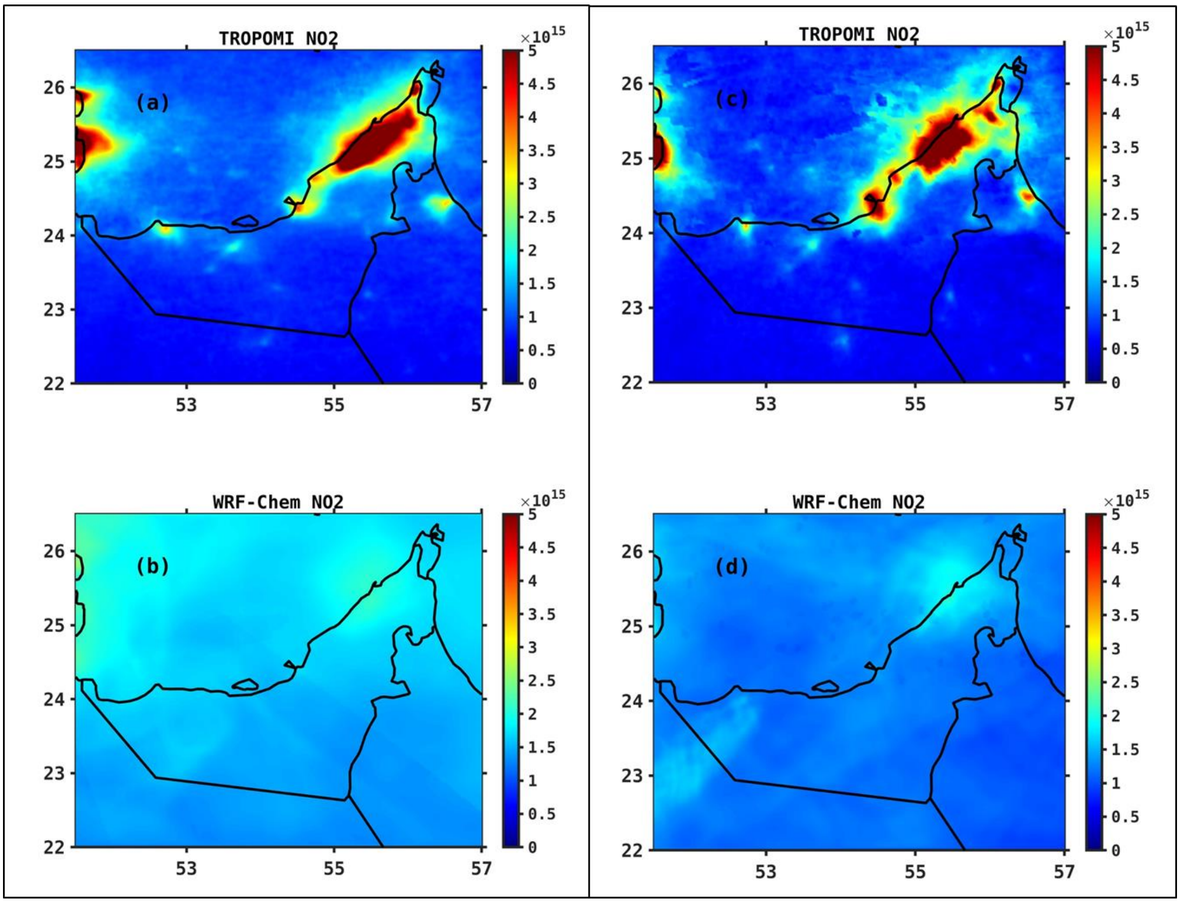


**Figure S4: The tropospheric column $NO_2$ from TROPOMI and WRF-Chem:** Spatial distribution of tropospheric column NO2 over the UAE as observed by TROPOMI and simulated by the WRF-Chem model during the summer (a,b) and winter (c,d) of 2022.

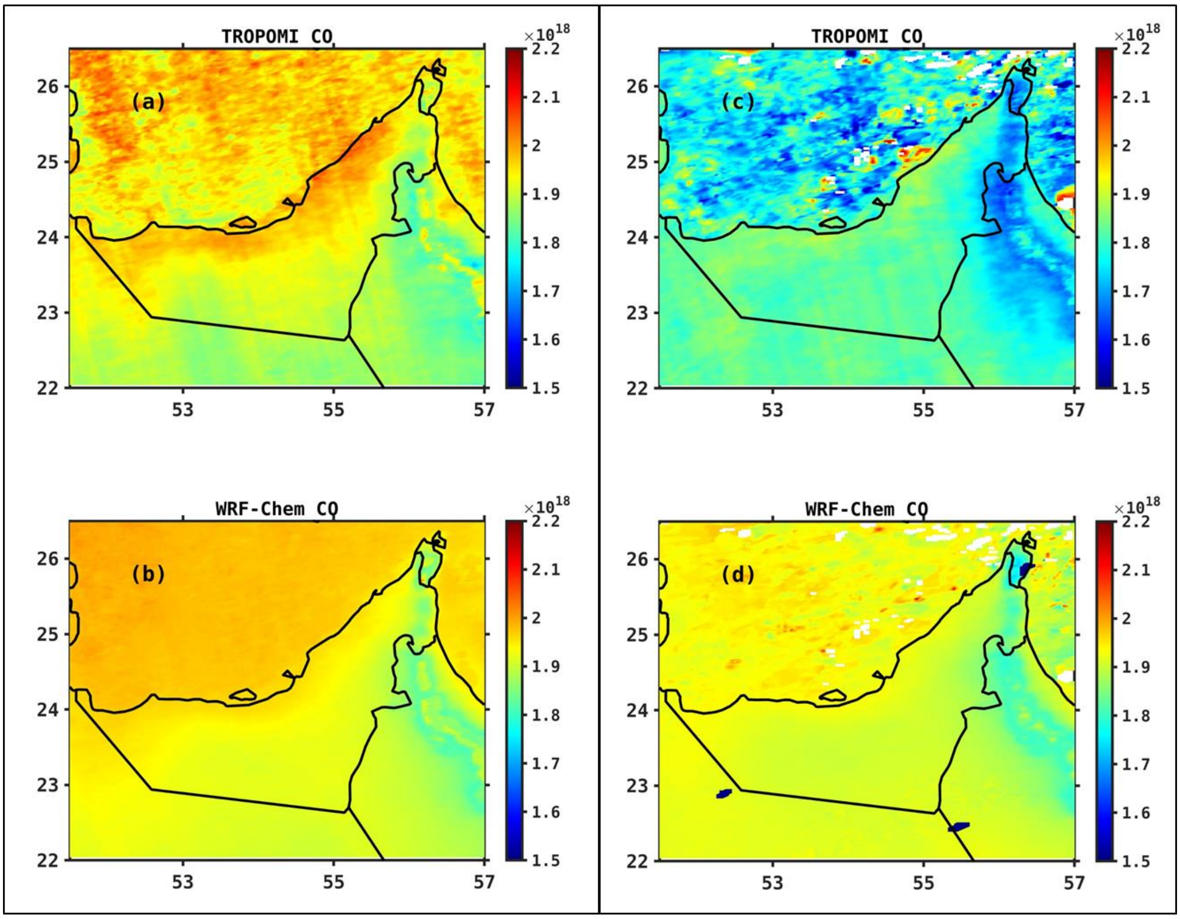


**Figure S5: The total column CO from TROPOMI and WRF-Chem:** Same as Fig. S4, but for total column CO.

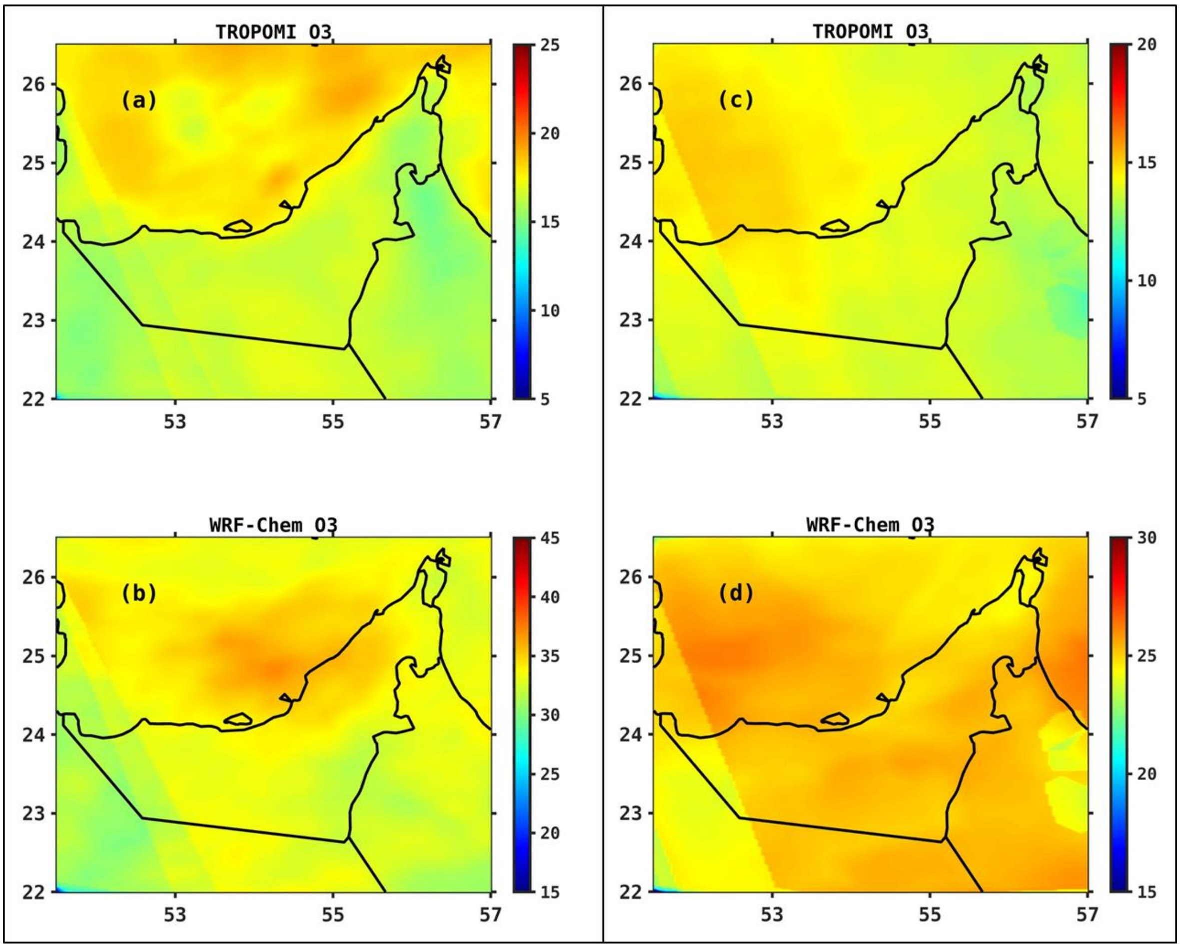


**Figure S6: The tropospheric column ozone from TROPOMI and WRF-Chem:** Similar to Figure S3, but for tropospheric column ozone. Note the differences in color scales between TROPOMI and WRF-Chem for both summer and winter.

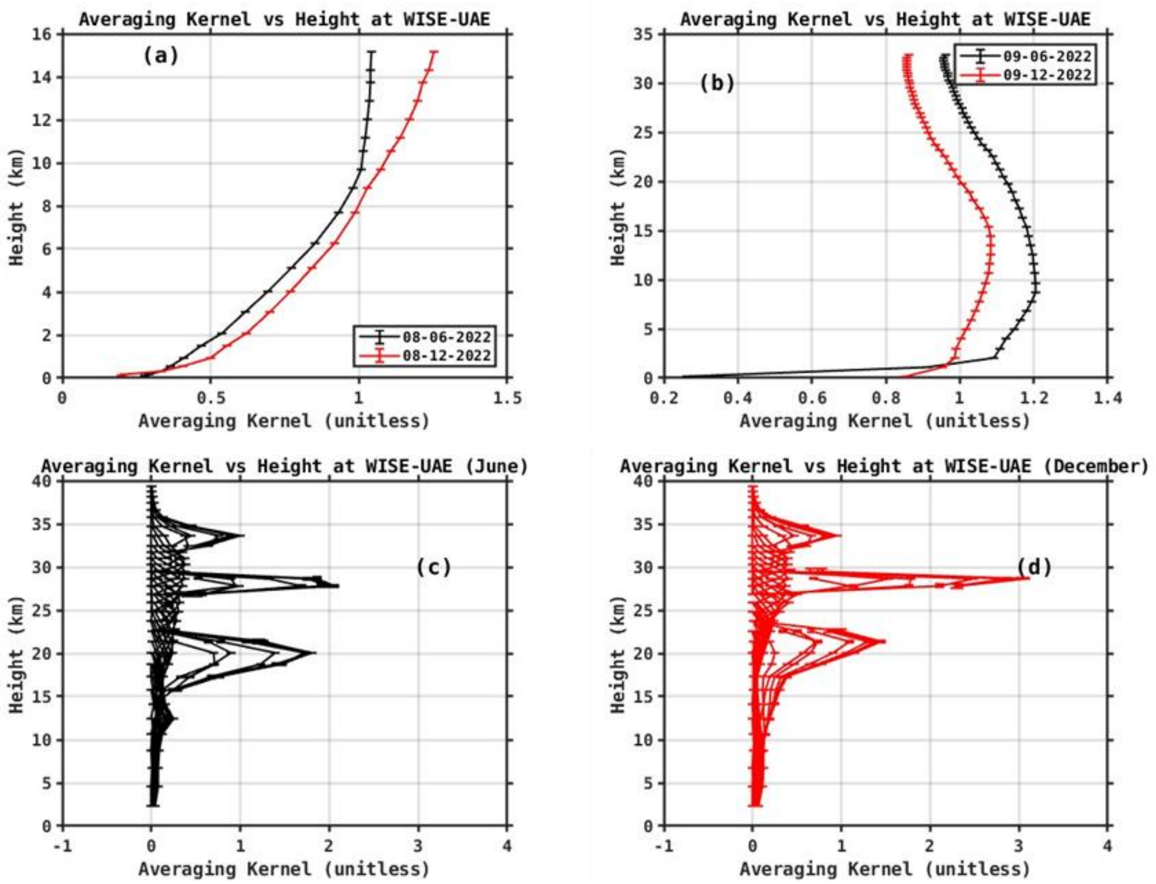


**Figure S7: The averaging kernel from TROPOMI:** (a) for tropospheric column $NO_2$ (example days for June (black) and December (red)). (b) for total column CO (example days for June (black) and December (red)), (c), and (d) for ozone averaging kernel profile for June and December, respectively. Note the differences in color scales.

# References


Abida, R., Addad, Y., Francis, D., Temimi, M., Nelli, N., Fonseca, R., Nesterov, O., & Bosc, E.: Evaluation of the Performance of the WRF Model in a Hyper-Arid Environment: A Sensitivity Study. *Atmosphere*, *13*(6). https://doi.org/10.3390/atmos13060985-2022, 2022.

Basha, G., Kishore, P., Ratnam, M. V., Ravindra Babu, S., Velicogna, I., Jiang, J. H., & Ao, C. O. (2019). Global climatology of planetary boundary layer top obtained from multi-satellite GPS RO observations. *Climate Dynamics*, *52*(3–4), 2385–2398. https://doi.org/10.1007/s00382-018-4269-1-2019, 2019.

Branch, O., Schwitalla, T., Temimi, M., Fonseca, R., Nelli, N., Weston, M., Milovac, J., & Wulfmeyer, V.: Seasonal and diurnal performance of daily forecasts with WRF V3.8.1 over the United Arab Emirates. *Geoscientific Model Development*, *14*(3), 1615–1637. https://doi.org/10.5194/gmd-14-1615-2021, 2021.

Chaouch, N., Temimi, M., Weston, M., & Ghedira, H.: Sensitivity of the meteorological model WRF-ARW to planetary boundary layer schemes during fog conditions in a coastal arid region. *Atmospheric Research*, *187*, 106-127. https://doi.org/10.1016/j.atmosres.2016.12.009-2017, 2017.

Chen, Y., Chen, S., Zhao, D., Li, J., Bi, H., Lou, G., & Guan, Y.: The role of boundary layer height in India on transboundary pollutions to the Tibetan Plateau. *Science of the Total Environment*, *837*. https://doi.org/10.1016/j.scitotenv.2022.155816-2022, 2022.

Fonseca, R., Temimi, M., Thota, M. S., Nelli, N. R., Weston, M. J., Suzuki, K., Uchida, J., Kumar, K. N., Branch, O., Wehbe, Y., Al Hosari, T., Al Shamsi, N., & Shalaby, A.: On the analysis of the performance of WRF and nicam in a hyperarid environment. *Weather and Forecasting*, *35*(3), 891–919. https://doi.org/10.1175/WAF-D-19-0210.1-2020, 2020.

Fonseca, R., Francis, D., Weston, M., Nelli, N., Farah, S., Wehbe, Y., Alhosari, T., Teixido, O., & Mohamed, R.: Sensitivity of summertime convection to aerosol loading and properties in the United Arab Emirates. *Atmosphere*, *12*(12). https://doi.org/10.3390/atmos12121687-2021, 2021.

Fonseca, R., Francis, D., Nelli, N., Farrah, S., Wehbe, Y., Al Hosari, T., & Al Mazroui, A.: Assessment of the WRF model as a guidance tool into cloud seeding operations in the United Arab Emirates. *Earth and Space Science*, *9*, e2022EA002269. https://doi.org/10.1029/2022EA002269-2022, 2022a.

Fonseca, R., Francis, D., Nelli, N., & Thota, M.: Climatology of the heat low and the intertropical discontinuity in the Arabian Peninsula. *International Journal of Climatology*, *42*(2), 1092–1117. https://doi.org/10.1002/joc.7291-2022, 2022b.

Francis, D., Temimi, M., Fonseca, R., Nelli, N. R., Abida, R., Weston, M., Wehbe, Y.: On the analysis of a summertime convective event in a hyperarid environment. *Quarterly Journal of the Royal Meteorological Society*, *147*, 501-525. https://doi.org/10.1002/qj.3930-2021, 2021.

Gopalakishnan, D., Taraphdar, S., Pauluis, O. M., Xue, L., Ajayamohan, R. S., Al Shamsi, N., Chen, S., Lee, J. A., Grabowski, W. W., Liu, C., Tessendorf, S. A., Rasmussen, R. M.: Anatomy of a Summertime Convective Event over the Arabian Region. *Monthly Weather Review*, *151*, 989-1004. https://doi.org/10.1175/MWR-D-22-0082.1-2023, 2023.

Kishta, M., Al Abadla, Z., Wahab, M. M. A., & Aldashti, H.: Assessment of Heat Wave Indexing and Performance of ERA5 in Simulating Temperature and Precipitation Dataset over the UAE. *Environment Asia*, *16*(2), 48–65. https://doi.org/10.14456/ea.2023.20-2023, 2023.

Nelli, N. R., Temimi, M., Fonseca, R. M., Weston, M. J., Thota, M. S., Valappil, V. K., Branch, O., Wulfmeyer, V., Wehbe, Y., Al Hosary, T., Shalaby, A., Al Shamsi, N., & Al Naqbi, H.: Impact of roughness length on WRF simulated land-atmospheres interactions over a hyper-arid region. *Earth and Space Science*, *7*, e2020EA001165. https://doi.org/10.1029/2020EA001165-2020, 2020.

Nelli, N., Fissehaye, S., Francis, D., Fonseca, R., Temimi, M., Weston, M., Abida, R., & Nesterov, O.: Characteristics of Atmospheric Aerosols Over the UAE Inferred From CALIPSO and Sun Photometer Aerosol Optical Depth. *Earth and Space Science*, *8*(6). https://doi.org/10.1029/2020EA001360-2021, 2021.

Nelli, N., Francis, D., Fonseca, R., Bosc, E., Addad, Y., Temimi, M., Abida, R., Weston, M., Cherif, C.: Characterization of the atmospheric circulation near the Empty Quarter Desert during major weather events. *Frontiers in Environmental Science*, *10*, 972380. https://doi.org/10.3389/fenvs.2022.972380-2022, 2022.

Nelli, N., Francis, D., Alkatheeri, A., & Fonseca, R.: Evaluation of Reanalysis and Satellite Products against Ground-Based Observations in a Desert Environment. *Remote Sensing*, *16*, 3593. https://doi.org/10.3390/rs16193593-2024, 2024.

Parajuli, S. P., Stenchikov, G. L., Ukhov, L., Morrison, H., Shevchenko, I., & Mostamandi, S.: Simulation of a Dust-And-Rain Event Across the Red Sea Using WRF-Chem. *Journal of Geophysical Research: Atmospheres* 128 (14). https://doi.org/10.1029/2022JD038384-2023, 2023.

Pauli, E., Cermak, J., Bendix, J., Stier, P.: Synoptic scale controls and aerosol effects on fog and low stratus life cycle processes in Po valley, Italy. *Geophysical Research Letters*, *51*, e2024GL111490. https://doi.org/10.1029/2024GL111490-2024, 2024.

Phanikumar, D. V., Basha, G., Ratnam, M. V., Kondapalli, N. K., Ouarda, T. B. M. K., Pangaluru, K.: Assessment of particulate matter concentration and gaseous pollutants in urban and rural regions over the Emirate of Abu Dhabi, UAE. *Journal of Atmospheric and Solar-Terrestrial Physics*, *199*, 105217. https://doi.org/10.1016/j.jastp.2020.105217-2020, 2020.

Schwitalla, T., Branch, O., & Wulfmeyer, V.: Sensitivity study of the planetary boundary layer and microphysical schemes to the initialization of convection over the Arabian Peninsula. *Quarterly Journal of the Royal Meteorological Society*, *146*(727), 846–869. https://doi.org/10.1002/qj.3711-2020, 2020.

Temimi, M., Fonseca, R., Nelli, N., Weston, M., Thota, M., Valappil, V., Branch, O., Wizemann, H., Kumar Kondapalli, N., Wehbe, Y., Hosary, T. AL, Shalaby, A., Shamsi, N. AL, & Naqbi, H. AL.: Assessing the Impact of Changes in Land Surface Conditions on WRF Predictions in Arid Regions. *Journal of Hydrometeorology*, 2829–2853. https://doi.org/10.1175/JHM-D-20-0083.1-2020, 2020.

Wang, Y., Bai, Y., Zhi, X., Wu, K., Zhao, T., Zhou, Y., Xiong, J., Zhu, S., Zhou, W., Hu, W., Zhang, L., & Meng, K.: Two Typical Patterns of Regional PM2.5 Transport for Heavy Air Pollution Over Central China: Rapid Transit Transport and Stationary Accumulation Transport. *Frontiers in Environmental Science*, *10*. https://doi.org/10.3389/fenvs.2022.890514-2022, 2022.

Wehbe, Y., Temimi, M., Weston, M., Chaouch, N., Branch, O., Schwitalla, T., Wulfmeyer, V., Zhan, X., Liu, J., Al Mandous, A.: Analysis of an extreme weather event in a hyper-arid region using WRF-Hydro coupling, station, and satellite data. Natural Hazards and Earth System Sciences, 19, 1129-1149. https://doi.org/10.5194/nhess-19-1129-2019, 2019.

Weston, M., Chaouch, N., Valappil, V., Temimi, M., Ek, M., Zheng, W. (2018) Assessment of the sensitivity to the thermal roughness length in Noah and Noah-MP land surface model using WRF in an arid region. *Pure and Applied Geophysics*, *176*, 2121-2137. https://doi.org/10.1007/s00024-018-1901-2-2018, 2018.

Yousef, A. L., Temimi, M., Molini, A., Weston, M., Wehbe, Y., Al Mandous, A. (2020) Cloud Cover over the Arabian Peninsula from Global Remote Sensing and Reanalysis Products. *Atmospheric Research*, *238*, 104866. https://doi.org/10.1016/j.atmosres.2020.104866-2020, 2020.